Investigating the contribution of grown new particles to cloud condensation nuclei with largely varying pre-existing particles - Part 2: Modeling chemical drivers and 3-D NPF occurrence

Ming Chu[1], Xing Wei[1], Shangfei Hai[1], Yang Gao[1,2*], Huiwang Gao[1,2], Yujiao Zhu[3], Biwu Chu[4], Nan Ma[5], Juan Hong[5], Yele Sun[6], Xiaohong Yao[1,2*]

[1]Frontiers Sci Ctr Deep Ocean Multispheres & Earth, Key Laboratory of Marine Environment and Ecology (MoE) and Sanya Oceanographic Institution, Ocean University of China, Qingdao, China

[2] Laboratory for Marine Ecology and Environmental Sciences, Qingdao National Laboratory for Marine Science and Technology, Qingdao, China

[3]Environment Research Institute, Shandong University, Qingdao 266237, China

[4]State Key Joint Laboratory of Environment Simulation and Pollution Control, Research Center for Eco-Environmental Sciences, Chinese Academy of Sciences, Beijing 100085, China

[5]Institute for Environmental and Climate Research, Jinan University, Guangzhou, 510000, China

[6]State Key Laboratory of Atmospheric Boundary Layer Physics and Atmospheric Chemistry, Institute of Atmospheric Physics, Chinese Academy of Sciences, Beijing, 100029, China

#Equally contributed to the study; **Correspondence to*: Yang Gao (yanggao@ouc.edu.cn) and Xiaohong Yao (xhyao@ouc.edu.cn)

Figure legends:

Fig. S1 Simulated concentrations of H_2SO_4 vapor on July 1–2 and the ranges of observational values reported in the literature (Two endpoints reported by Lu et al. (2019) and Wang et al. (2021) represent the maximum and minimum values, respectively).

Fig. S2 Diurnal variations in modeled chemical components in 10–40 nm particles and 40–250 nm particles: (a) SO_4^{2-}, (b) NO_3^-, (c) NH_4^+ (d) organics on July 3–4; fractions of chemical species in 10–40 nm particles at 15:00 (e), in 40–250 nm particles at 15:00 (f), in 10–40 nm particles at 22:00 (g), and in 40–250 nm particles at 22:00 on July 3.

Fig. S3 The simulated chemical components in 10–40 nm particles at 500 m, 1500 m and 2500 m above the ground at 10:00 (a), 15:00 (b), 22:00 (c) on July 3 and 3:00 (d) on July 4.

Fig. S4 Horizontal distributions of CN_{10} at ~1300 m a.s.l. (a, the upper row) and on the ground level (a, the bottom row) at 08:00, 09:00, 12:00, 17:00 and 18:00 on July 3, 2019 (red and blue solid dots represent the observational site and point A, respectively; the direction and length of black arrow represent the wind direction and wind speed, respectively); Vertical profiles of CN_{10} over the observation site (red solid line) and point A (blue dashed line) from 0:00 to 22:00 on 3 July 2019 (b, the Y-axis coordinate is the height above the ground; the red and blue solid dots represent the height of the PBL over the observational site and point A, and PBL exceeding 3000 meters above the ground are not shown in Figure).

Fig. S5 Horizontal distribution of CN_{10} at ~1300 m a.s.l. (a, the upper row) and on ground (a, the bottom row) in NPF event occurred on July 6, 2019 at 10:00, 11:00, 14:00, 17:00 and 18:00 (the red and blue solid dots represent the observation site and point A, respectively; the direction and size of the black arrow represent the wind direction and wind speed, respectively); Vertical profiles of CN_{10} over the observational site (red solid line) and point A (blue dashed line) from 0:00 to 22:00 on July 6, 2019 (b, the Y-axis coordinate is the height above the ground; the red and blue solid dots represent the height of the PBL over the observational site and point A, and PBL exceeding 3000 meters above the ground are not shown in Figure).

Fig. S6 Horizontal distribution of $CN_{40–250}$ on ground (a, the upper row) and vertical profiles of $CN_{40–250}$ over the observational site (red solid line), point A (blue dashed line) and point B (black dashed line) from 18:00 on July 3 to 04:00 on July 4 (b, the Y-axis coordinate is the height above the ground; the red, blue and black solid dots represent the height of the PBL over the observational site, point A and point B, and PBL exceeding 3000 meters above the ground are not shown in Figure).

Table legends:

Table S1. Parameter scheme setting in WRF-Chem model

Figures

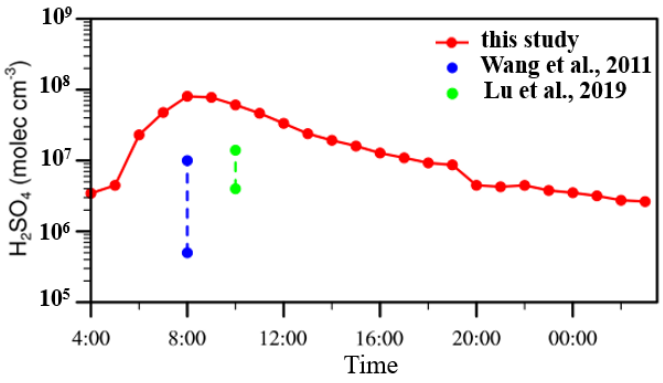

Fig. S1

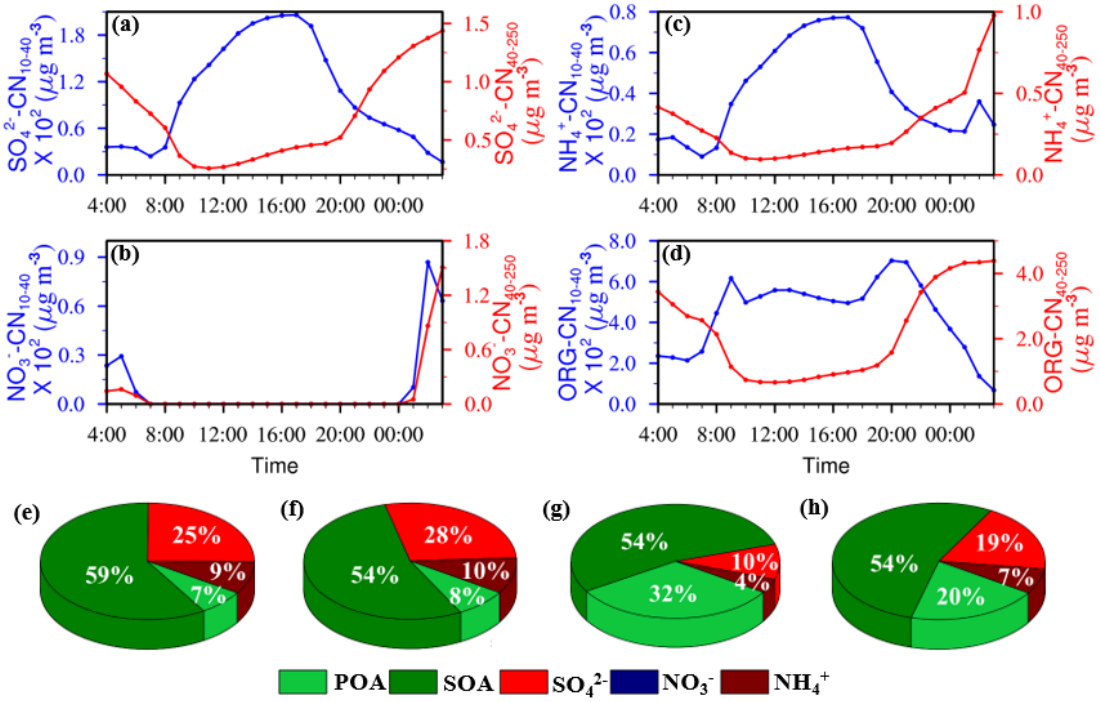
(a)
(b)
(c)
(d)
Time
Time
4:00 8:00 12:00 16:00 20:00 00:00
(e)
25%
9%
7%
59%
(f)
28%
10%
8%
54%
(g)
54%
10%
4%
32%
(h)
19%
7%
20%
54%
POA
SOA
SO4 2-
NO3-
NH4+

Fig. S2

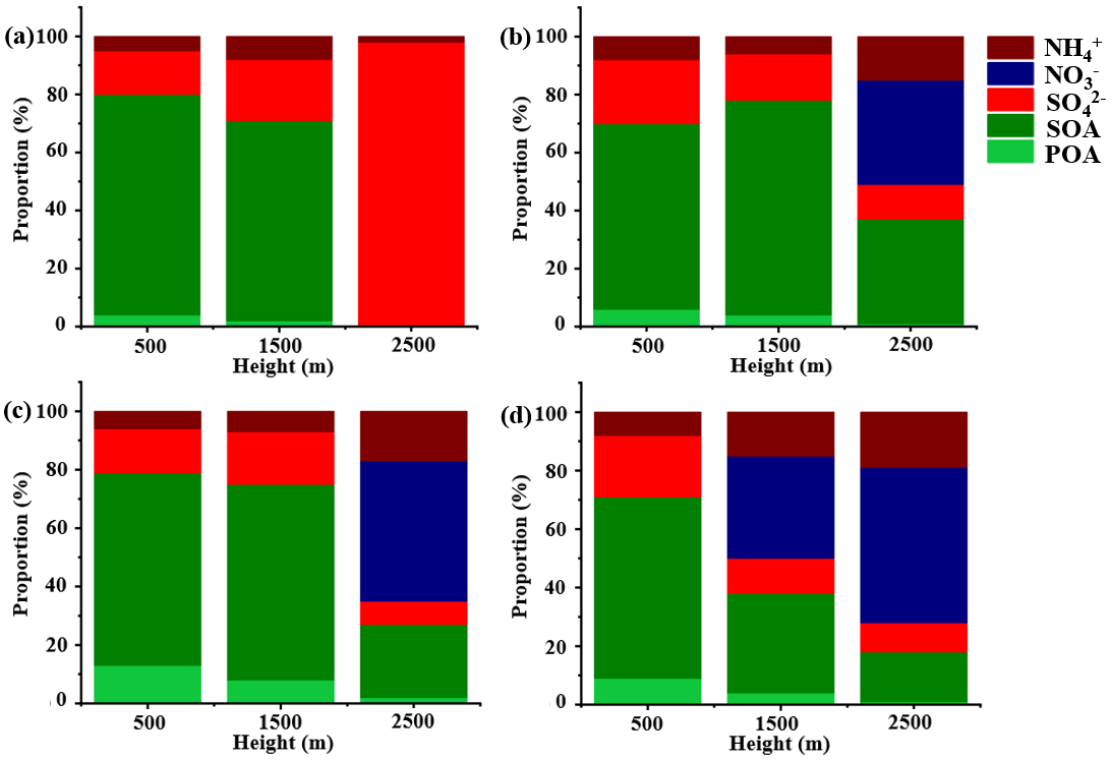
(a)
(b)
(c)
(d)
Proportion (%)
Height (m)
500
1500
2500
0
20
40
60
80
100
NH4+
NO3-
SO42-
SOA
POA

Fig. S3

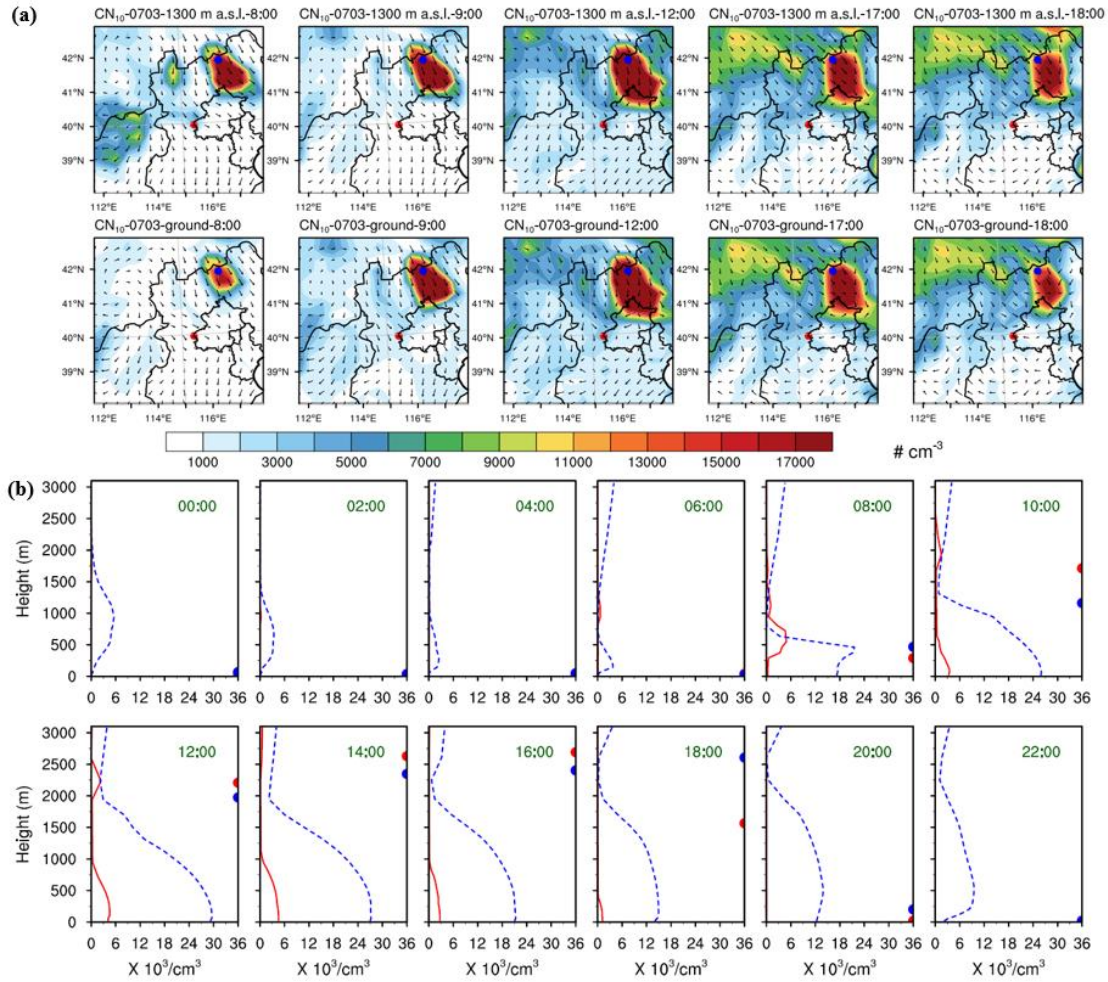
(a)
CN10-0703-1300 m a.s.l.-8:00
CN10-0703-1300 m a.s.l.-9:00
CN10-0703-1300 m a.s.l.-12:00
CN10-0703-1300 m a.s.l.-17:00
CN10-0703-1300 m a.s.l.-18:00
CN10-0703-ground-8:00
CN10-0703-ground-9:00
CN10-0703-ground-12:00
CN10-0703-ground-17:00
CN10-0703-ground-18:00
42°N
41°N
40°N
39°N
112°E
114°E
116°E
1000
3000
5000
7000
9000
11000
13000
15000
17000
cm-3
(b)
Height (m)
00:00
02:00
04:00
06:00
08:00
10:00
12:00
14:00
16:00
18:00
20:00
22:00
0
500
1000
1500
2000
2500
3000
0 6 12 18 24 30 36
X 10^3/cm^3

Fig. S4

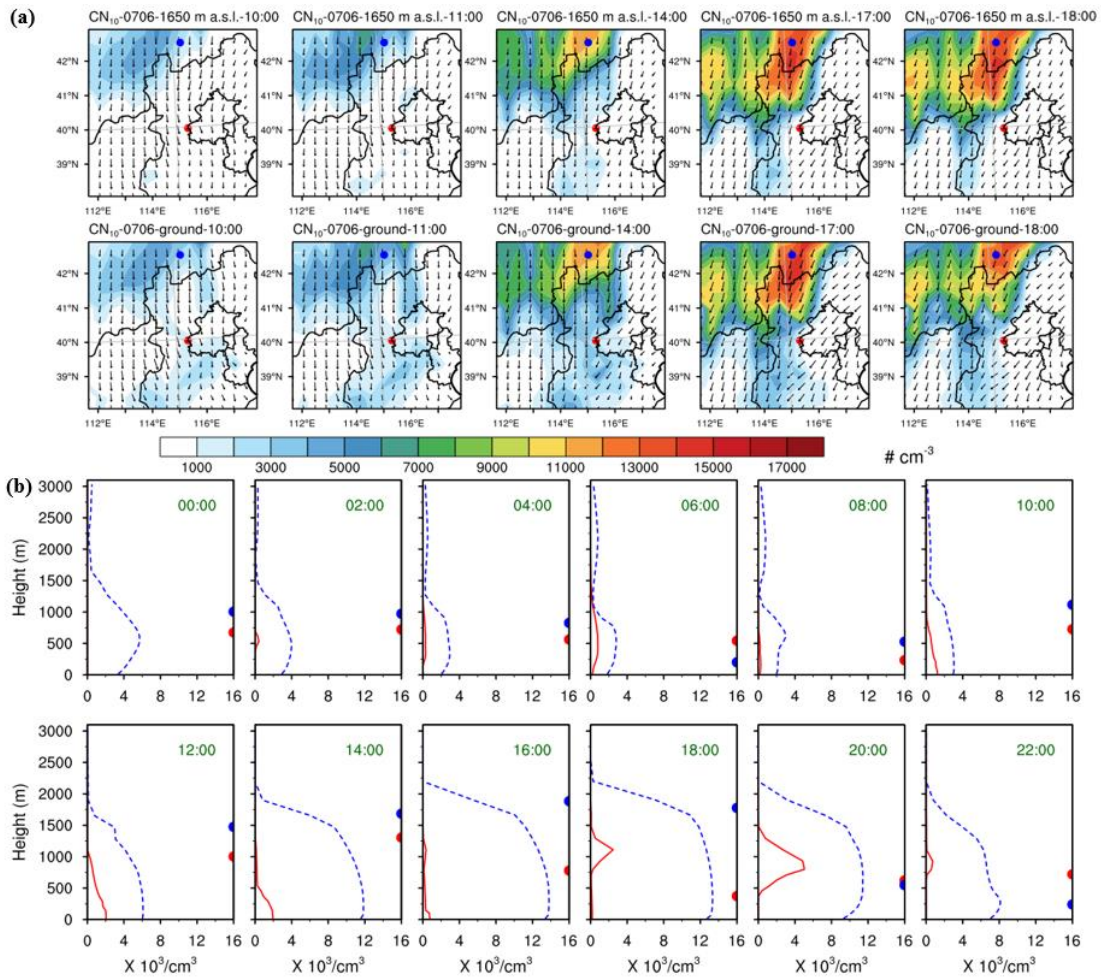
(a)
CN10-0706-1650 m a.s.l.-10:00
CN10-0706-1650 m a.s.l.-11:00
CN10-0706-1650 m a.s.l.-14:00
CN10-0706-1650 m a.s.l.-17:00
CN10-0706-1650 m a.s.l.-18:00
CN10-0706-ground-10:00
CN10-0706-ground-11:00
CN10-0706-ground-14:00
CN10-0706-ground-17:00
CN10-0706-ground-18:00
42°N
41°N
40°N
39°N
112°E
114°E
116°E
1000
3000
5000
7000
9000
11000
13000
15000
17000
cm-3
(b)
Height (m)
00:00
02:00
04:00
06:00
08:00
10:00
12:00
14:00
16:00
18:00
20:00
22:00
X 10^3/cm^3

Fig. S5

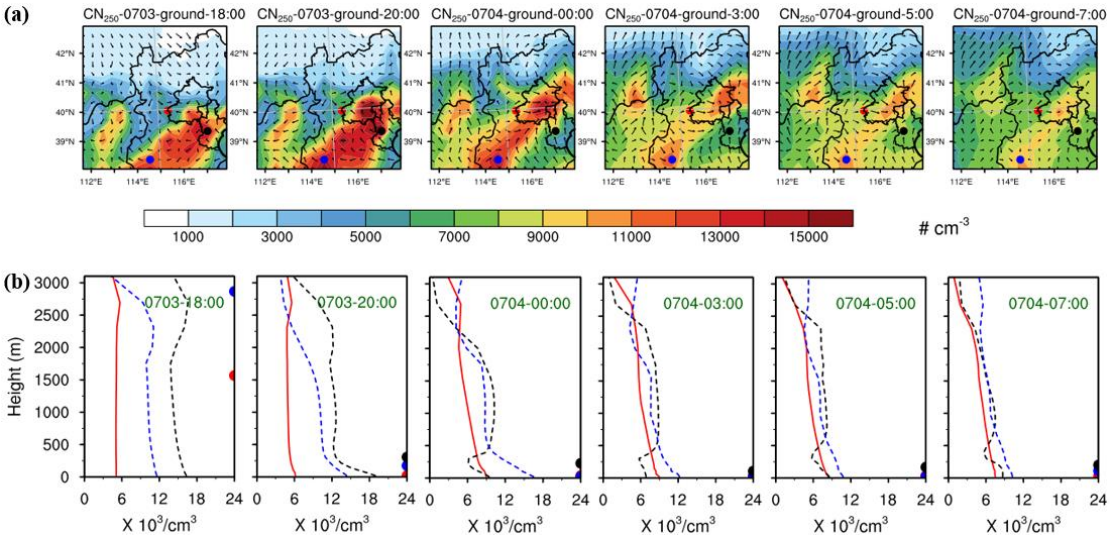
(a)
CN250-0703-ground-18:00
CN250-0703-ground-20:00
CN250-0704-ground-00:00
CN250-0704-ground-3:00
CN250-0704-ground-5:00
CN250-0704-ground-7:00
42°N
41°N
40°N
39°N
112°E
114°E
116°E
1000
3000
5000
7000
9000
11000
13000
15000
cm-3
(b)
Height (m)
3000
2500
2000
1500
1000
500
0
0703-18:00
0703-20:00
0704-00:00
0704-03:00
0704-05:00
0704-07:00
0
6
12
18
24
X 10^3/cm^3

Fig. S6

Table

Table S1 Parameter scheme setting in WRF-Chem model

Atmospheric process	Model scheme
Meteorological process	
Longwave radiation	RRTMG (Iacono et al., 2008)
Shortwave radiation	RRTMG (Iacono et al., 2008)
Land surface model	Unified Noah LSM (Tewari et al., 2016)
PBL scheme	YSU (Tewari et al., 2016)
Cumulus	Grell 3D (Grell and Dévényi, 2002)
Micro Physics	Morrision 2-moment (Morrison et al., 2009)
Chemical process	
Gas-phase chemistry	SAPRC99 (Carter, 2000)
Photolysis	Madronich F-TUV (Madronich, 1987)
Aerosol chemistry	MOSAIC (Zaveri et al., 2008)
Anthropogenic emissions	Modified MEIC2016
Biogenic emissions	MEGAN v2.03

References

Carter, W.: Additions And Corrections To The Saprc-99 Maximum Incremental Reactivity (mir) Scale, 2000. Grell, G. A., and Dévényi, D.: A generalized approach to parameterizing convection combining ensemble and data assimilation techniques, Geophys. Res. Lett., 29, 38-31-38-34, https://doi.org/10.1029/2002GL015311, 2002.

Iacono, M. J., Delamere, J. S., Mlawer, E. J., Shephard, M. W., Clough, S. A., and Collins, W. D.: Radiative forcing by long-lived greenhouse gases: Calculations with the AER radiative transfer models, J. Geophys. Res., 113, D13103, https://doi.org/10.1029/2008JD009944, 2008.

Lu, Y. Q., Yan, C., Fu, Y. Y., Chen, Y., Liu, Y. L., Yang, G., Wang, Y. W., Bianchi, F., Chu, B. W., Zhou, Y., Yin, R. J., Baalbaki, R., Garmash, O., Deng, C. J., Wang, W. G., Liu, Y. C., Petaja, T., Kerminen, V. M., Jiang, J. K., Kulmala, M., and Wang, L.: A proxy for atmospheric daytime gaseous sulfuric acid concentration in urban Beijing, Atmos. Chem. Phys., 19, 1971-1983, 10.5194/acp-19-1971-2019, 2019.

Madronich, S.: Photodissociation in the atmosphere: 1. Actinic flux and the effects of ground reflections and clouds, J. Geophys. Res., 92, 9740-9752, https://doi.org/10.1029/JD092iD08p09740, 1987.

Morrison, H., Thompson, G., and Tatarskii, V.: Impact of Cloud Microphysics on the Development of Trailing Stratiform Precipitation in a Simulated Squall Line: Comparison of One- and Two-Moment Schemes, Mon. Weather. Rev., 137, 991-1007, https://doi.org/10.1175/2008MWR2556.1, 2009.

Tewari, M., Chen, F., Wang, W., Dudhia, J., and Cuenca, R. H.: Implementation and verification of the united NOAH land surface model in the WRF model, 20th Conference on Weather Analysis and Forecasting/16th Conference on Numerical Weather Prediction, 2016.

Wang, Z. B., Hu, M., Yue, D. L., Zheng, J., Zhang, R. Y., Wiedensohler, A., Wu, Z. J., Nieminen, T., and Boy, M.: Evaluation on the role of sulfuric acid in the mechanisms of new particle formation for Beijing case, Atmos. Chem. Phys., 11, 12663-12671, 10.5194/acp-11-12663-2011, 2011.

Zaveri, R. A., Easter, R. C., Fast, J. D., and Peters, L. K.: Model for Simulating Aerosol Interactions and Chemistry (MOSAIC), J. Geophys. Res. Atmos., 113, https://doi.org/10.1029/2007JD008782, 2008.